OPEN ACCESS
IOP Publishing
Plasma Physics and Controlled Fusion
Plasma Phys. Control. Fusion **66** (2024) 125016 (9pp)
https://doi.org/10.1088/1361-6587/ad8fd0

Millimetre wave super pulses mediated by multidimensional structured surfaces

A J MacLachlan*, A D R Phelps, C W Robertson, P MacInnes, C G Whyte and K Ronald

Department of Physics, University of Strathclyde, Glasgow G4 0NG, United Kingdom

E-mail: amy.maclachlan@strath.ac.uk

Received 28 July 2024, revised 18 October 2024
Accepted for publication 7 November 2024
Published 21 November 2024

Abstract

The need to bridge the THz gap is stimulated by a growing number of important applications including biochemical spectroscopy, plasma turbulence diagnostics and drive sources for tokamaks. Cherenkov sources based on two-dimensional (2D) corrugated surface lattice interaction structures, in which the diameter is several times greater than the radiation wavelength, hold strong promise to bridge the THz gap. In this paper, we demonstrate the ability to drive these sources, typically intended for steady-state operation, into the highly non-linear superradiant regime. We demonstrate, for the first time, the ability to generate superradiant pulses, for which the peak power scales as the number of electrons in the bunch squared, by exploiting slippage of an electron beam through subluminal surface waves close to the metallic 2D corrugation. The surface waves are scattered into low order, forward propagating $TM_{0,N}$ modes which form the emitted 'super pulse'. To drive superradiance, the nanosecond electron bunch must have a fast rising edge with a suitably high (kiloamperes) electron current. Superradiant pulses have been simulated for cases where the relative difference between the group speed of the electromagnetic wave and the drift speed of the electron beam is in the correct range. We show that, for this transient process, the diameter-to-wavelength ratio of the interaction cavities can be scaled from 6 to 9, with a corresponding uplift in peak power from 450 MW to 750 MW, demonstrating the potential for exceptionally powerful THz pulses. The presented results have been obtained for a Cherenkov maser operating in the 83–94 GHz range. However, numerical dispersion analysis, validated by full-wave simulations, shows the potential to radically modify the wave dispersion by varying the 2D lattice geometry for highly controllable, powerful signals at any frequency from 1 GHz to 1 THz. Based on these results, the capability to eventually generate gigawatt-level pulses in the THz range can be projected.

Keywords: Cherenkov, high-power microwaves, mm-wave, non-linear electrodynamics, surface wave oscillator, superradiance

* Author to whom any correspondence should be addressed.

1. Introduction

Research in the field of high-power, high-frequency source development is motivated by the need to close the 'terahertz-gap' (0.1–1 THz) for important applications relevant to plasma physics and magnetically confined fusion. Terahertz waves at the lower end of the spectrum are a promising way to deliver energy and in particular to drive current in magnetically confined fusion plasmas, fuelling the demand for highly efficient, megawatt-level, continuous-wave (CW) sources as required for fusion initatives. With the move towards industrial systems, capable of large-scale energy production, the plasma density and confining magnetic field, and consequently the target frequency of the drive sources, is likely to increase >0.2 THz.

Moreover, sources with enhanced power capabilities in the higher THz range would support the development of high resolution, multi-channel plasma diagnostics—providing coherent, powerful signals that can be discerned in inherently noisy hot plasma environments—for future fusion power plants. In addition to these applications in fusion science, powerful (pulsed and CW) sub-THz and THz sources are needed for advanced radar systems, remote sensing, non-destructive testing and biochemical spectroscopy i.e. enhanced nuclear magnetic resonance using dynamic nuclear polarisation and high-field electron paramagnetic resonance (EPR).

Challenges in the realisation of high-power sub-THz and THz sources are attributable to various factors. These include: the lack of output power (milliwatts to hundreds of milliwatts) offered by solid state sources which tend to require complex chains of multipliers; the dearth of quantum transitions in the THz domain, and the miniaturisation (at shorter wavelengths) of the electronic circuitry of backward-wave oscillators.

In the latter, the reduced interaction volume—which increases the risk of RF breakdown and limits the output power $P \sim 1/f^2$—is imposed by the requirement for the transverse interaction size to scale with the free-space wavelength λ in order to preserve the phase and spectral coherence of the output radiation.

Studies have uncovered new possibilities to overcome this disadvantageous power scaling by increasing the transverse interaction region dimension with respect to λ, while simultaneously implementing a novel mode control and selection method to ensure coherent, stable operation [1–15]. This entails the use of periodic surface lattices based on cylindrical (or possibly planar [11, 12]) waveguides.

Such lattices, composed of sub-wavelength two-dimensional (2D) corrugations, can suppress the excitation of parasitic modes in very oversized, and therefore highly overmoded, interaction cavities, through the resonant coupling of high-order volume and surface waves to form a dominant coupled, cavity eigenmode [1, 3, 9, 10, 13]. As the structures become more overmoded, the steady-state conditions for the formation of the hybrid coupled cavity eigenmode (with both E_z and H_z field components) required for coherent single-frequency emission, become increasingly stringent. The structures can be described according to their oversize parameter,

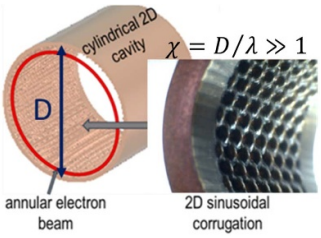

Figure 1. Diagram showing oversized 2D lattice interaction cavity of radiation source based on a Cherenkov interaction between the coupled eigenmode and an annular electron beam.

$\chi = D/\lambda$ where D is the diameter of the cylindrical interaction cavity. For cylindrical interaction structures, as shown in figure 1, the co-sinusoidal corrugation on the inner wall is defined:

$$r = r_0 + \Delta r \cos\left(\bar{m}\varphi\right)\cos\left(\bar{k}_z z\right)$$

where r_0 is the mean radius, Δr is the corrugation amplitude, $\bar{m}$ is the number of azimuthal periods around the circumference of the cylinder, and $\bar{k}_z = 2\pi/d_z$ is the lattice wavevector, defined by the axial periodicity, d_z.

Coherent radiation can be generated by the Cherenkov interaction between the eigenmode of the oversized cylindrical interaction cavity (figure 1) and a thin, annular electron beam, propagating close to the corrugated cavity wall. For cylindrical surface lattices with $\chi = 3.5$, multi-megawatt pulses at frequencies of ∼0.35 THz [9] have been predicted. It has subsequently been shown that the structures are scalable, both in frequency and transverse size [10] and that, although the limit in χ has not yet been reached, the potential for CW operation at powers of up to a megawatt are feasible [13]. Such sources offer potential benefits (lower magnetic guide field, higher output power at frequencies above 0.2 THz and superior overall efficiency when combined with a novel energy recovery system [13]) as compared with existing microwave source technologies, including state-of-the-art fusion gyrotrons.

The use of these 2D lattices in overmoded radiation sources is attracting increasing interest [1–15]. However, due to the complexity of the 2D lattices, in comparison to one-dimensional (1D) corrugated structures which are widely used in applications, the potential of these novel sources to provide the power levels and frequency control demanded by applications, remains relatively untapped. In this paper, we report exciting indications that oversized Cherenkov sources based on 2D surface lattices, can be driven into the highly nonlinear superradiative regime for which exceptional levels of peak power, and instantaneous efficiency, are attainable. By studying the fundamental differences in the nonlinear dynamics of the steady-state and superradiant regimes, an in-depth understanding of the collective relativistic electrodynamics, vital to the development of new THz technologies, can be established.

The term 'superradiance' was conceived in 1954 by Dicke to describe coherent photon emission from a gas [16]. A defining feature of superradiance is that the signal strength is directly proportional to the number of oscillators squared. Similar observations, beyond the strict definition of Dicke superradiance, have since led to the term being more broadly used in atomic physics, quantum mechanics, astrophysics and free electron physics to describe radiation enhancement processes with similar scaling. The study of superradiance in free electron lasers [17–20], in particular, shares many conceptual similarities with superradiance in a Cherenkov maser [21–27].

Superradiative emission in a Cherenkov maser operating at ∼35 GHz and based on an $\chi \sim 1$, 1D corrugated interaction structure was demonstrated experimentally in the 1990's [21, 22]. To drive this regime, it was shown that the slippage of the electrons relative to the electromagnetic wave, determined by the difference in the group speed of the wave v_g and the drift velocity v_z of the electrons, must be in the correct range. Critically, the current of the driving beam, and therefore the gain, must be high (typically several kiloamps) and sufficiently short in duration (as defined in section 2) with a sharp leading edge as a seed for the superradiant emission and a fast falling edge.

When these conditions are satisfied, a soliton-like electromagnetic pulse drifts through the electron beam (or vice versa depending on whether $v_g > v_z$ or $v_g < v_z$) absorbing free electron energy and spatially decoupling from the electrons before conventional saturation can arise, and compressing the accumulated energy into a short duration, powerful 'super pulse' at the falling edge of the electron macro bunch. Analogous to the classical Dicke superradiance, the emitted power scales as the square of the electron current, with an intensity proportional to n_e^2 where n_e is the electron number density of the driving pulse.

Historically, $\chi \sim 1$, 1D Cherenkov masers have exhibited strong superradiance for a phase synchronous backward wave coupling (i.e. where v_g is negative, or at least less than v_z) [22, 23]. In this paper, we show the potential for forward wave slippage interactions using surface lattices with 2D corrugations. With a few notable exceptions [14, 15], studies of overmoded Cherenkov sources based on 2D lattices have focussed predominantly on the steady-state regime. Here, we demonstrate the additional dispersion and mode control offered by these 2D lattices in the highly non-linear superradiant regime, with strong promise for the eventual realisation of gigawatt levels of peak power at high frequencies. Much of the novelty of this work lies in the highly overmoded nature and complexity of the 2D surface lattice interaction structures that mediate the superradiant emission. In this paper we demonstrate, for the first time, that this transient maser regime can operate at a preferred frequency when the oversize parameter is signifcantly increased from $\chi = 6$–9. The observation of superradiance in this highly overmoded $\chi = 9$ scenario has major implications for the future development of pulsed THz sources where high χ values are required to mitigate breakdown. Moreover, the majority of research has, until now, focused on backward wave slippage interactions. In this paper, we investigate transient interactions exploiting the slippage of an electron beam through a relatively slower forward propagating electromagnetic wave.

2. Theory: coupled electromagnetic fields in the transient regime

The 2D surface lattice with subwavelength features is electromagnetically equivalent to an 'effective metadielectric'. The field structure inside the cylindrical surface lattice interaction structure can therefore be described by deriving the fields within a smooth cylindrical waveguide lined with a thin dielectric. The hybrid surface field has both axial electric E_z and magnetic H_z field components, which are defined separately within the two media (dielectric and vacuum) each with different permittivities. The boundary conditions $E_z = 0$ and $\frac{\partial}{\partial r} H_z = 0$ are imposed at the metallic wall. At the lattice boundary ($r = r_w$), the axial field components are written:

$$E_{z,1} = C_1 \left[\left(J_m \left(k_\perp^s r \right) Y_m \left(k_\perp^s r_w \right) - Y_m \left(k_\perp^s r \right) J_m \left(k_\perp^s r_w \right) \right) \right] \times \sin \left(\bar{m} \varphi \right) \exp \left(i \bar{k}_z z \right) \quad (1a)$$

$$H_{z,1} = C_2 \left[\left(J_m \left(k_\perp^s r \right) Y'_m \left(k_\perp^s r_w \right) - Y_m \left(k_\perp^s r \right) J'_m \left(k_\perp^s r_w \right) \right) \right] \times \cos \left(\bar{m} \varphi \right) \exp \left(i \bar{k}_z z \right) \quad (1b)$$

where m is the azimuthal index of the surface mode, $\bar{m}$ is the number of azimuthal periods of the lattice, $C_{1,2,3,4}$ are amplitude constants, J_m and Y_m are Bessel functions of the first and second kind and J'_m and Y'_m are their derivatives. Near the centre of the waveguide, the rapidly decaying surface field with $k_\perp^{s'} = \sqrt{\bar{k}_z^2 - k^2}$ is described using a modified Bessel function, $I_m \left(k_\perp^{s'} r \right)$:

$$E_{z,2} = - \left(k_\perp^{s'} \right)^2 C_3 \left(I_m \left(k_\perp^{s'} r \right) \right) \sin \left(\bar{m} \varphi \right) \exp \left(i \bar{k}_z z \right) \quad (2a)$$

$$H_{z,2} = - \left(k_\perp^{s'} \right)^2 C_4 \left(I_m \left(k_\perp^{s'} r \right) \right) \cos \left(\bar{m} \varphi \right) \exp \left(i \bar{k}_z z \right). \quad (2b)$$

The tangential field components in the two regions can be derived from equations (1) and (2) [1]. To ensure continuity of the tangential field and impedance matching at the lattice interface ($r = r_w$) the following boundary constraints are imposed: $E_{z,1} = E_{z,2}$; $H_{z,1} = H_{z,2}$; $E_{\varphi,1} = E_{\varphi,2}$; $H_{\varphi,1} = H_{\varphi,2}$. This analysis pertains to the hybrid fields (with both E_z and H_z components) within the surface lattice interaction region. Beyond the corrugation, the hybrid surface field is scattered into the propagating azimuthally symmetric transverse magnetic volume waves that form the emitted 'super pulse'. This method is valid for both the steady-state and superradiant regimes and the dispersion can be derived as described in [1]. One key difference in the analysis of these two regimes is the azimuthal field structure of the surface field and the length of the electron bunch, l_e.

In traditional spontaneous coherent emission, the bunch of electrons is shorter than the radiation wavelength enabling the electrons to emit coherently with an intensity directly proportional to the number of particles in the bunch squared. However, in the 1980s, an intermediate regime in which the bunch is longer than the wavelength but still much shorter than the length required for 'quasi-CW' operation, was discovered. Of fundamental importance, when considering the electron bunch length in these superradiant masers, is the cooperation length l_c; defined as the relative slippage distance between the radiation envelope and the electron pulse in one gain length:

$$l_c \approx l_z \left(1 + \frac{v_z}{v_g}\right). \tag{3}$$

Here, l_z is the length of the interaction space. Ideally, for superradiance, the cooperation length should be greater than, or at least comparable to, the electron bunch length, l_e which in turn should be much larger than the radiation wavelength, i.e. $\lambda \ll l_e \leq l_c$.

3. Simulation of superradiant cherenkov masers based on periodic structures

Numerical modelling has been undertaken using the Particle-in-Cell (PiC) and eigenmode solvers of CST Studio Suite. Preliminary studies were carried out to verify the validity of the PiC model for a superradiant Cherenkov maser based on a $\chi \sim 1$, 35 GHz, 1D corrugated interaction structure with identical parameters (interaction region and electron bunch) to those of earlier laboratory experiments [21, 22]. Direct comparison of the simulated and measured powers is complicated by the use of explosive emission annular cathodes in the experiments, which impacted on the beam transport and alignment. Another complicating factor is that the measured peak power in the experiments was likely underesitmated due to the short nanosecond pulses challenging the frequency response and calibration of the 27–40 GHz detectors available at the time [21, 22]. Nevertheless, the CST PiC simulations produce frequencies, mode patterns, and power as a function of time envelope shapes consistent with the experiments in [22], validating the numerical PiC model.

With contemporary simulation tools, it is now possible to explore the complicated nonlinear electrodynamics and electromagnetic coupling mechanisms, extending these studies to consider superradiance in Cherenkov sources based on 2D lattice interaction structures. The superradiant process is illustrated schematically in figure 3. The sharp edge of the extended (short) electron beam 'macro bunch' initially emits the seed for the forward and backward propagating EM waves, amplifying and compressing the wave into a short duration 'super pulse' at the trailing edge of the macro bunch. The 2D corrugation is tapered at the input and output ends of the structure as shown in figure 2. To reduce the computation time, a simplified injection scheme consisting of a planar annular emitter and thin grid as described in [9] has been implemented.

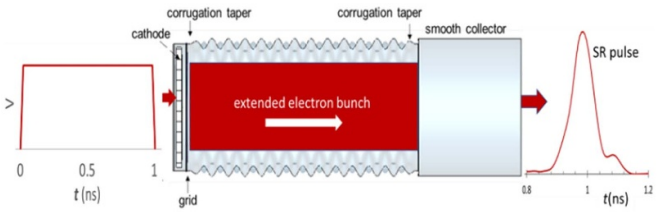

Figure 2. Schematic illustration of superradiant process and 2D surface lattice interaction structure.

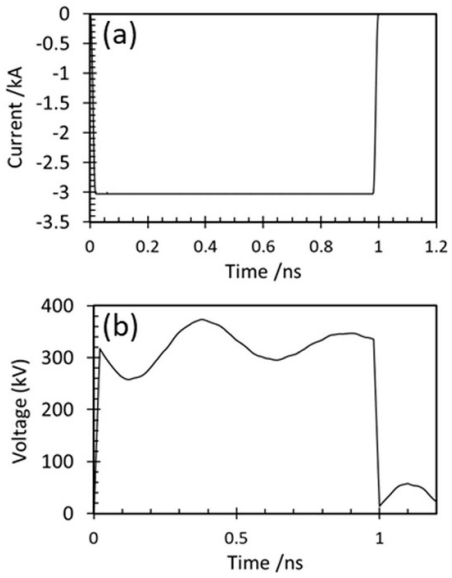

Figure 3. (a) nanosecond current pulse with sharp rise and fall times and (b) oscillation in the voltage input pulse due to the impedance mismatch.

The impedance of the transmission line is set low to ensure the cathode emitter is able to accept and supply a very large (several kiloamps) current injection.

The simulated 1 ns, 3 kA current pulse is presented in figure 3(a). These Cherenkov masers exploit a well-known technique for transporting very high currents by injecting a thin annular beam very close to the conducting cavity wall in the presence of a strong magnetic guiding field. In this scenario, the current is far below its limiting value, greatly reducing the risk of undesirable beam instabilities.

Due to the impedance mismatch of the external port impedance to the electron gun impedance, the amplitude of the electron beam power is varying during the input electrical pulse as shown in figure 3(b). In similar devices, magnetically insulated diodes utilising cold explosive emission cathodes [14, 28] have been used to supply kiloamperes of current with rapid rise and fall times. Future experiments demonstrating the concepts presented in this paper could exploit a sharpened graphite knife-edge to produce the desired nanosecond kiloampere electron beam with a rise time of 10 s of picoseconds. To ensure that the beam is injected sufficiently close to the

interaction cavity wall, the effects of plasma expansion will need to be carefully managed.

4. Numerical dispersion study

The 2D lattice interaction structures are similar to those simulated in [9, 10, 13] and can be fabricated using additive manufacturing [4] or copper electrodeposition onto precision-machined aluminium formers [3] with good results reported at relatively high frequencies of around 0.35 THz [29]. However, due to fundamental differences in the nonlinear electrodynamics of the steady-state and superradiant regimes, the optimal geometrical lattice parameters and dispersive properties, vary significantly. The lattices have been designed for operation at frequencies just below the lower threshold of the terahertz (0.1–10 THz) range. This is particularly attractive for applications due to the atmospheric window at ∼94 GHz. Since the scalability of these interaction regions has already been proven, at least in the steady-state regime [10], operation well into the THz range can be extrapolated. The 'cold' numerical dispersions for the $TM_{0,N}$ modes, calculated using the CST Eigenmode Solver and normalised by the axial lattice wavevector $\bar{k}_z$, are presented in figures 4–6. The solid black line is the electron beam with an accelerating potential of 330 kV.

Figure 4(a) shows the dispersion curves for the $TM_{0,N}$ modes where $N = 1,\ldots,6$. The low order $TM_{0,1}$ and $TM_{0,2}$ modes are excited below the light line (dashed lines) when $k_z/\bar{k}_z \sim 0.2$–0.8 and $k_z/\bar{k}_z \sim 0.3$–0.7 respectively [30]. In these regions, the evanescent modes, which converge near the π-point, exist purely as surface waves. The interaction with the 330 kV electron beam at ∼94 GHz is also predicted to occur near the π-point, providing mode selection due to the especially subluminal group velocity and the relatively high coupling impedance of the low order surface modes. For comparision, the dispersion of the equivalent 1D lattice (with identical parameters except for its azimuthal uniformity, $\bar{m} = 0$) is presented figure 4(b). It is observed that, due to the lower predicted interaction frequency, the oversize parameter is effectively lower, $\chi \sim 3.6$.

Figure 5 shows the $TM_{0,1}$ dispersion curves of the $\chi = 5.5$ lattice with decreasing azimuthal and axial period. The solid red, green and blue lines respresent lattices with $d_z = 1.20$ mm and $\bar{m} = 16$, 20, 32 respectively while the dotted purple line corresponds to the case where $\bar{m} = 16$, $d_z = 0.60$ mm. As expected, the predicted interaction frequency increases with $\bar{m}$, with the $TM_{0,1}$ mode existing purely as a surface wave. This same effect cannot be replicated by reducing d_z, for which the $TM_{0,1}$ mode is evansecent only in the immediate vicinity of the π-point ($k_z/\bar{k}_z = 0.45$–0.55) justifying the utility of the azimuthal corrugation for certain interactions.

Increasing $\bar{m}$ represents a key difference in the fundamental mode selection mechanism as compared to the steady-state sources [9, 10, 13] in which $\bar{m}$ is fixed to match the azimuthal index of the desired (high azimuthal order) surface field, closest in frequency to the near cut-off (high radial order) volume field. It is presently unclear whether such high-order coupled eigenmodes can be established in the transient superradiant regime and, while this is intuitively expected to depend on the signal transit time around the circumference of the

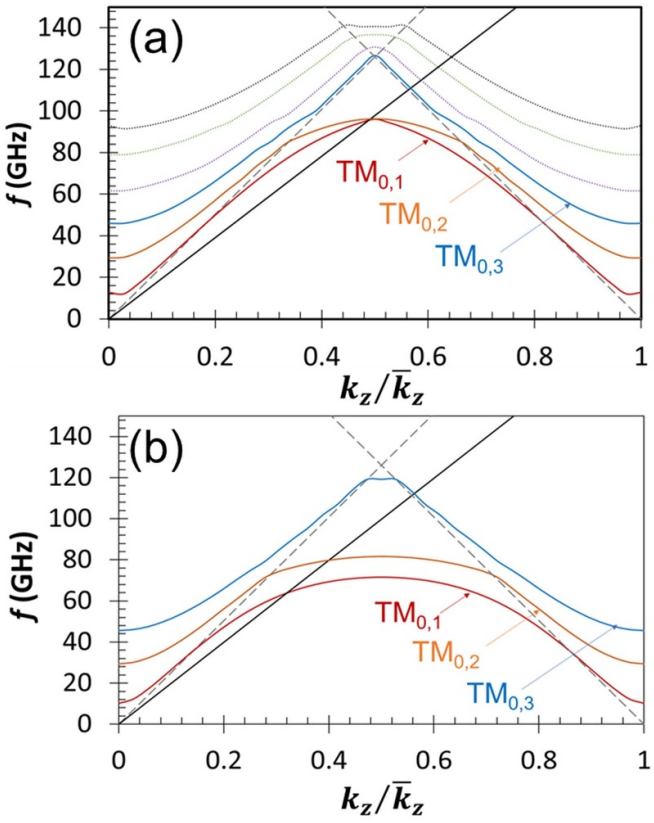

Figure 4. Numerical dispersion for the $TM_{0,N}$ modes of the (a) $\chi = 5.5$ 2D lattice with parameters: $r_0 = 9$ mm, $\Delta r = 0.54$ mm, $\bar{m} = 16$, $d_z = 1.20$ mm. The $TM_{0,1}$, $TM_{0,2}$, $TM_{0,3}$, $TM_{0,4}$, $TM_{0,5}$, and $TM_{0,6}$ modes are represented by the red, orange, blue, purple (dotted), green (dotted) and black (dotted) curves respectively. The dispersion curves for the $TM_{0,1-3}$ modes of the $\chi = 2$, 1D lattice ($r_0 = 9$ mm, $\Delta r = 0.54$ mm, $\bar{m} = 0$, $d_z = 1.20$ mm) are shown in (b). The black lines represent electron beams with an accelerating potential of 330 kV.

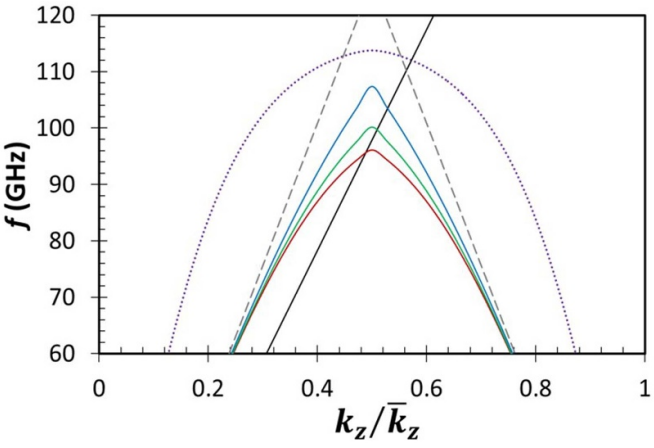

Figure 5. Numerical dispersion diagram for the $TM_{0,1}$ mode of the $\chi = 5.5$, 2D lattice with $d_z = 1.20$ mm, $\bar{m} = 16$, 20, 32 (red, green, blue curves) and $\bar{m} = 16$, $d_z = 0.60$ mm (dotted purple curve).

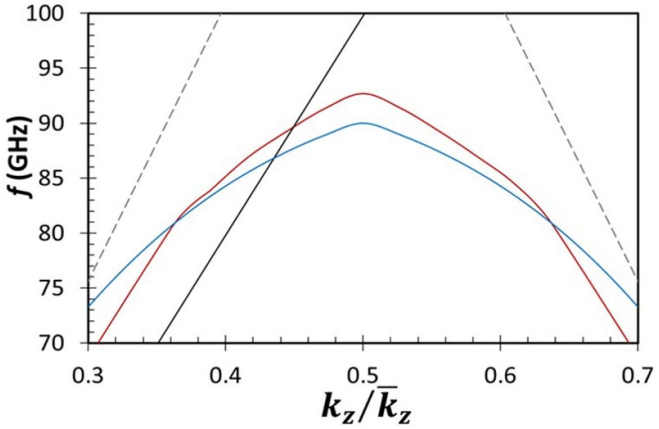

Figure 6. Numerical TM_{01} mode dispersions for (i) $\chi = 5.5$, $r_0 = 9.00$ mm, $\bar{m} = 32$, $d_z = 1.20$ mm, Δr =0.75 mm (red curve) and (ii) $\chi = 9$, $r_0 = 16.00$ mm, $\bar{m} = 32$, $d_z = 1.00$ mm, $\Delta r = 0.70$ mm cylindrical 2D surface lattice interaction structures.

Table 1. Parameters of lattice interaction structures and electron beam corresponding to the dispersion diagrams and PiC simulation results in figures 4, 6–13.

r_0 (mm)	Δr (mm)	$\bar{m}$	d_z (mm)	n	V (Kv)	I(kA)	l_e(cm)	Dispersion/figure	PiC/figure
9	0.54	16	1.20	32	330	3.0	24	4(a)	8,9,10
9	0.75	32	1.20	32	330	3.0	24	6	11,12
16	0.70	32	1.00	64	330	5.2	24	7	13

large-diameter structures, other determining factors likely include the rise time of the electron bunch and the lattice corrugation depth.

Increasing the corrugation depth Δr enhances the electrodynamic gain. However, one of the challenges, when targetting a particular frequency, is the marked downshift in frequency with increasing Δr. The red dispersion curve in figure 6 represents the TM_{01} mode of a χ =5.5, $\bar{m}$ =32, $d_z = 1.20$ mm, Δr =0.75 mm 2D lattice. Higher peak power at the preferred excitation frequency can be generated by decreasing the azimuthal periodicity while simultaneously increasing Δr. The dispersion predicts slippage of the electron beam through a forward propagating wave with a relatively slow group velocity. Similarly, the blue curve (figure 6) shows the TM_{01} mode of a $\chi \sim 9$ 2D lattice with $r_0 = 16$, $\bar{m}$ =32, $d_z = 1.00$ mm, Δr =0.70 mm.

The dispersion predicts the potential to increase the radius while maintaining single-frequency output just below the lower THz threshold range by exploiting an interaction with the forward propagating wave, slightly farther from but still close to, the π-point. The wave is predicted to have a higher group velocity, and therefore smaller v_z/v_g, requiring a longer interaction structure to ensure adequate slippage. Demonstrating the scaling of χ for this transient maser regime, confrims the eventual potenital to generate extremely powerful pulses.

5. PiC results: 2D overmoded sources

Full-wave simulations have been undertaken using the PiC solver of CST Particle Studio to study the complex electrodynamics. Table 1 lists the parameters of all three simulated cases and links them to their predicted dispersions. The electron phase space plots showing the electron energy as a function of axial position for the $\chi = 5.5$ Cherenkov maser are presented in figure 7. When the group velocity of the EM wave is sufficiently different to the electron drift velocity, the amplification mechanism is fundamentally different to that of the steady-state. The plots show the self-amplification and stimulated micro-bunching of the electrons in the macro electron bunch of radiation, produced initially by the electrons at the leading edge of the pulse, through a process known as Self amplified coherent spontaneous emission. In this process, the front of the wave is amplified by unmodulated electrons. As the wave rapidly accumulates energy from the electrons, then after a certain slippage distance, the peak electromagnetic power greatly exceeds that of the spontaneous emission. In conventional travelling wave tubes, phase trapping occurs as the electrons lose energy and drop out of synchronism with the wave [9, 10, 13]. In this transient regime, the relative difference in the group speed of the wave and the electron drift velocity causes a slippage effect, resulting in a spatial decoupling which mitigates the usual saturation mechanism.

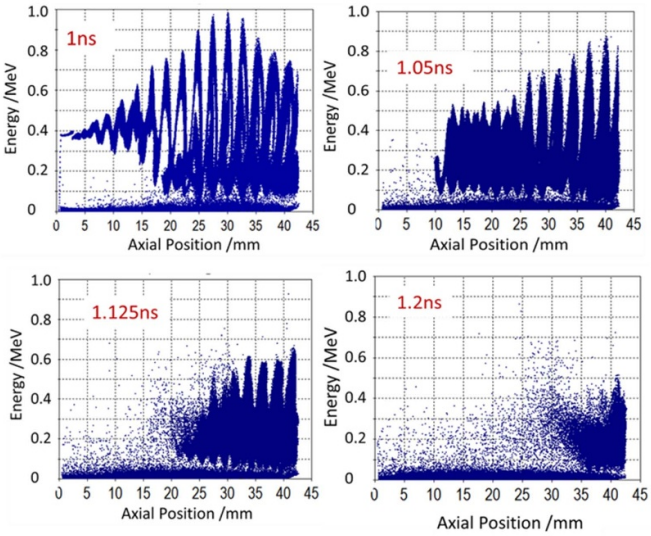

Figure 7. Electron phase space plots at times, $t = 1.00$ ns, 1.05 ns, 1.125 ns and 1.20 ns. In addition to the high energy electron population at 330 kV, a relatively weak, low energy population exists as an artefact of the simplified injection model used to minimise the simulation volume. This population is not resonant with the electromagnetic wave and has no impact on the microwave generation observed.

The simulated power in the $TM_{0,N}$ modes ($N = 1.3$) for a Cherenkov maser based a 2D lattice with $\chi = 5.5$, $d_z = 1.20$ mm and $\bar{m}$ =16 driven by a $I = 3$ kA, $V = 330$ kV beam is shown in figure 8. A super pulse, composed of $TM_{0,N}$ waves, is emitted at the falling edge of the electron macro bunch at a frequency of ∼93 GHz in agreement with the dispersion diagram in figure 4(a). As expected, the majority of the output power (>170 MW) is in the $TM_{0,1}$ mode. The total radiated peak power is 220 MW, giving an instantaneous efficiency of 22%. Simulations of the equivalent 1D case ($\bar{m}$ =0) exhibit relatively weaker peak power (∼100 MW) predominantly in the $TM_{0,1}$ mode and radiated at ∼60 GHz, demonstrating good spectral agreement with figure 4(b) and showing the possible benefits, in terms of frequency control and power, of the more complicated 2D geometry [30]. It should be noted, however, that neither the 1D nor 2D lattice interaction structures have been optimised.

For the 2D case, the cooperation length is comparable to the pulse length $l_c \sim l_e$, providing adequate slippage of the electrons through the wave. Figure 9(a) shows the dependence of the super pulse peak amplitude on the electron pulse duration for the case of a constant beam current. The radiated peak power plotted as a function of the pulse duration is similar to that of the experimentally measured superradiative emission in [22, 26]. Figure 9(b) demonstrates a near-linear dependence of the peak output power on the number of electrons in the bunch squared, confirming that the peak radiated power is directly proportional to n_e^2, as characteristic of superradiance.

Similar to the 1D experiments in [20–22] which were operated either single pulse or at pulse repetition frequencies of ∼100 Hz, simulations indicate that it is also possible to efficiently utilize a given source of primary energy by operating these oversized superradiant sources based on 2D lattices in the repetitively pulsed, short pulse regime. Figure 10 shows the power radiated in the dominant $TM_{0,1}$ mode over a series of repetitions [30].

As predicted from the numerical dispersion analysis, the radiated peak power can be substantively increased by halving the azimuthal periodicity ($\bar{m}$ =32) while simultaneously

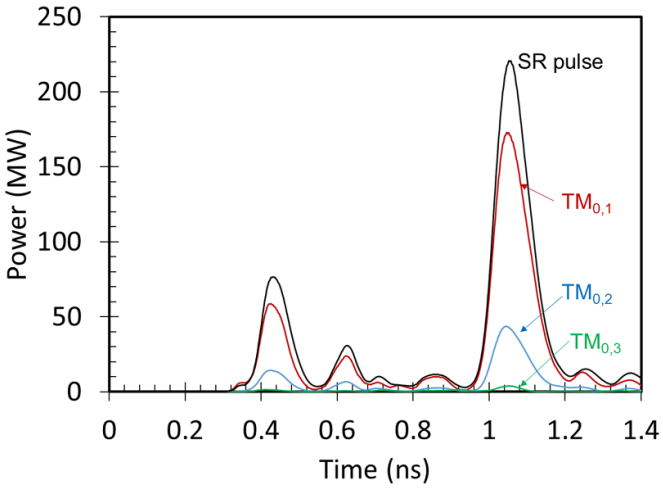

Figure 8. Power in 'super pulse' composed of $TM_{0,1}$, $TM_{0,2}$ and $TM_{0,3}$ modes for a Cherenkov maser based a 2D lattice with χ =5.5 and $\bar{m}$ =16, Δr=0.54 mm.

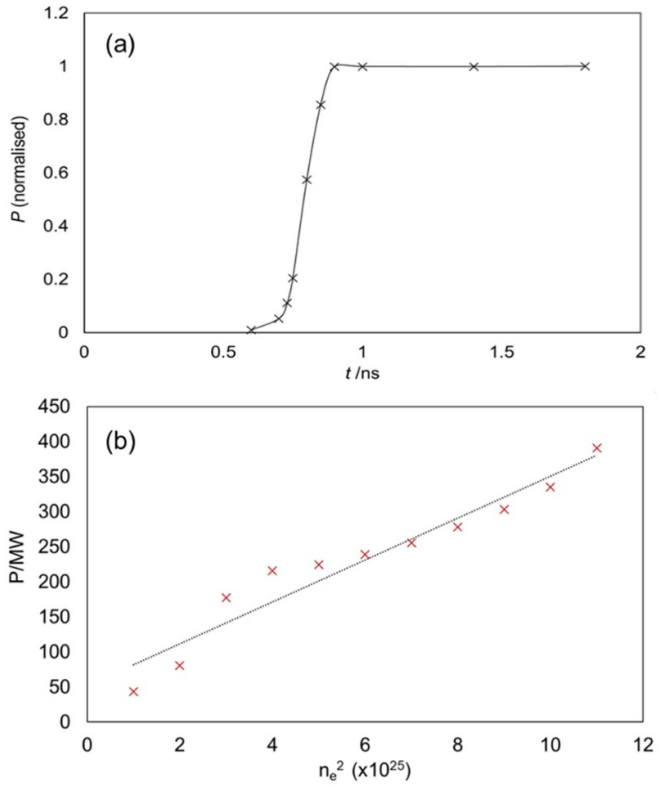

Figure 9. (a) Normalised peak power as a function of the electron bunch duration in nanoseconds showing a near square law in the region $t \sim 0.6$–0.8 ns. (b) Peak power (in megawatts) as a function of the number of electrons in the bunch squared. As characteristic of superradiance, $P \propto n_e^2$.

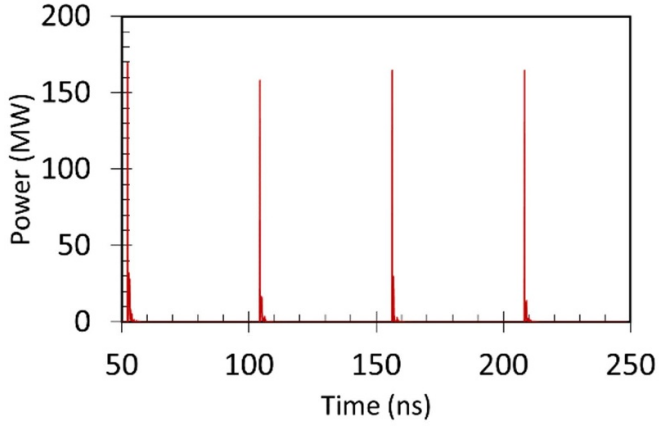

Figure 10. Power radiated in dominant $TM_{0,1}$ mode for cherenkov maser based on 2D lattice operating in repetitively pulsed short pulse regime.

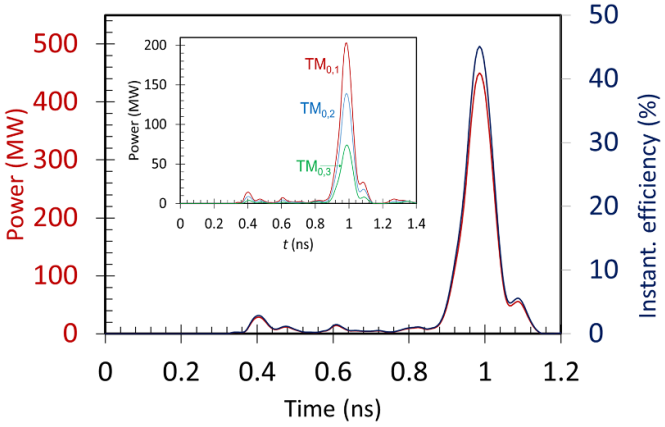

Figure 11. Total radiated peak power in super pulse of Cherenkov maser based a 2D lattice with $\chi = 5.5$ and $\bar{m} = 32$, $\Delta r = 0.75$ mm. (left) and instantaneous efficiency (right). The power radiated in the $TM_{0,N}$ ($N = 1.3$) modes forming the super pulse is shown inset.

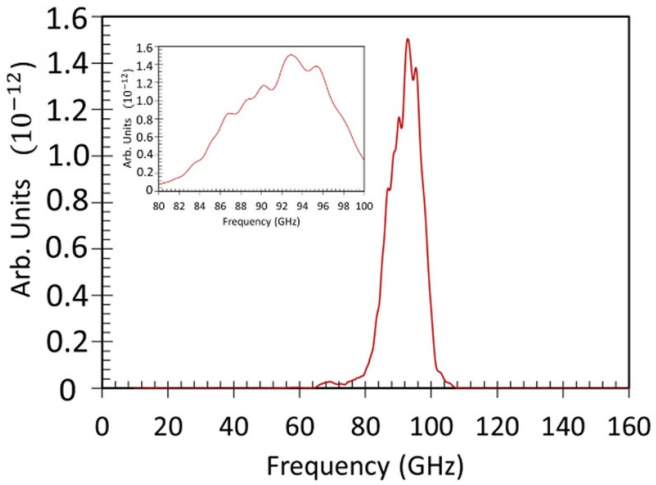

Figure 12. Spectral plot showing the spread spectrum emission at 94 GHz [30].

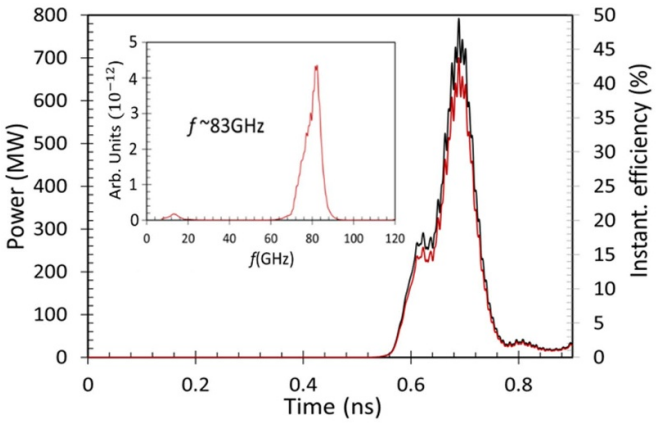

Figure 13. Radiated power and spectral plot (inset) for Cherenkov maser based on a grossly oversized ($\chi \sim 9$) 2D lattice interaction cavity.

increasing the corrugation depth, Δr=0.75 mm. Figure 11 shows a total >450 MW of radiated peak power in the super-mode composed of $TM_{0,N}$ ($N = 1.3$) modes with the power in each mode given inset. Here, the cooperation length $l_c \sim$18 cm is slightly less than the electron bunch length, suggesting that strong superradiance can be observed just below the threshold values calculated from equation (3).

The corresponding spectral plot is presented in figure 12. Clearly, the short duration of the emitted pulses increases the frequency bandwidth giving rise to a spread spectrum output. The radiated frequency shows good agreement with that predicted from the numerical dispersion in figure 6.

The ability to increase the radius while retaining the desired output frequency, i.e. increasing the oversize parameter χ, has significant importance for the generation of exceptionally powerful, high frequency pulses. Figure 13 shows >700 MW of peak power at 83 GHz, simulated for a Cherenkov maser with r_0 =16 mm and $\chi \sim$9. Due to the long computation time, the source and lattice interaction cavity have not been fully optimised. However, the potential to eventually generate gigawatt-class power at any given frequency is clear.

In figure 13 the superradiant pulse is formed at $t = 0.7$ ns; significantly sooner than the time (t =1.0 ns) at which the main pulse, emitted at the trailing edge of the electron bunch, is observed in figures 9 and 11. This can be attributed to the different slippage conditions arising from the forward wave slippage (further from the π-point) and the longer interaction structure. The PiC results demonstrate the ability to control the timing of the superradiant emission by adjusting the precise slippage conditions.

6. Conclusions

In this paper, super pulses composed of low order $TM_{0,N}$ modes, delivering hundreds of megawatts of output power in the mm-wave range, have been simulated by exploiting slippage of the electrons with respect to a forward propagating electromagnetic wave. Good spectral agreement between

the numerical dispersions and the full-wave PiC- simulations has been demonstrated. The presented results, for which the peak power is proportional to the number of electrons in the bunch squared, are highly charateristic of superradiance. Until now, few studies have focused on forward wave superradiance, and the simulation of superradiant emission in a Cherenkov maser based on a highly overmoded 2D interaction cavity, for which the diameter is nearly 9 times the radiation wavelength, is considered an important breakthrough. The oversized geometry and forward-wave slippage have signficant importance for the future scaling of these devices to higher frequencies. Backward-wave devices often utilise reflectors, prone to RF breakdown, especially in small-scale tubes. These oversized forward-wave devices offer advantageous frequency scaling by cirmumventing this challenge. A major outcome of this work is the confirmation that, even in this highly non-linear transient regime, the transverse dimension of the interaction region is scalable (from 9 mm to 16 mm) for a given frequency. The limit in the diameter to wavelength ratio has not yet been established but, based on these results, gigawatt-class output powers can be projected. The capacity for good temporal and spectral control of these superradiant pulses using novel oversized multi-dimensional interaction cavities has been established. Although the overall energy efficiency remains $<100\%$, due to the internal 'pulse compression' effect of the slippage process, $>100\%$ instantaneous efficiency may eventually be achieved by understanding the complex electrodynamics and fully optimising the control parameters of these novel superradiant masers. Future experiments will require a thin annular electron beam with a suitably fast rising edge injected very close to the interaction cavity wall. Field emission can be achieved using a sharpened graphite knife edge. In practice, achieving the required beam and alignment will be challenging, with the effects of plasma expansion needing to be closely monitored.

Data availability statement

The data that support the findings of this study are openly available at the following URL/DOI: https://doi.org/10.15129/e5d23ee5-4208-4428-83a2-69494c39a459.

Acknowledgment

The authors gratefully acknowledge support from the Air Force Office of Scientific Research (AFOSR) through Grant FA 8655-22-1-7251.

ORCID iDs

A J MacLachlan https://orcid.org/0000-0002-8960-1683
A D R Phelps https://orcid.org/0000-0002-1100-1012
C W Robertson https://orcid.org/0000-0002-3552-466X
P MacInnes https://orcid.org/0000-0003-2882-9817
C G Whyte https://orcid.org/0000-0002-5431-2443
K Ronald https://orcid.org/0000-0002-8585-0746

References

[1] Konoplev I V, MacLachlan A J, Robertson C W, Cross A W and Phelps A D R 2011 *Phys. Rev.* A **84** 1
[2] Ginzburg N S, Malkin A M, Sergeev A S and Zaslavsky V Y 2012 *Appl. Phys. Lett.* **100** 14
[3] Konoplev I V, MacLachlan A J, Robertson C W, Cross A W, Phelps A D R and Ronald K 2012 *Appl. Phys. Lett.* **101** 12
[4] Phipps A R, MacLachlan A J, Robertson C W, Zhang L, Konoplev I V, Cross A W and Phelps A D R 2016 *Nucl. Instrum. Methods Phys. Res.* B **402** 202–5
[5] Ginzburg N S, Ilyakov E V, Kulagin I S, Malkin A M, Peskov N Y, Sergeev A S and Zaslavsky V Y 2018 *Phys. Rev. Accel. Beams* **21** 8
[6] MacLachlan A J, Robertson C W, Konoplev I V, Cross A W, Phelps A D R and Ronald K 2019 *Phys. Rev. Appl.* **11** 034034
[7] MacLachlan A J, Robertson C W, Cross A W, Ronald K and Phelps A D R 2020 *IET Microw. Antennas Propag.* **14** 11
[8] Malkin A M, Zheleznov I V, Sergeev A S and Ginzburg N S 2021 *Phys. Plasmas* **28** 6
[9] MacLachlan A J, Robertson C W, Cross A W and Phelps A D R 2022 *IEEE Trans. Electron Devices* **69** 11
[10] MacLachlan A J, Robertson C W, Cross A W and Phelps A D R 2023 *IEEE Trans. Electron Devices* **70** 6
[11] MacLachlan A J, Robertson C W, Cross A W and Phelps A D R 2018 *AIP Adv.* **8** 05115
[12] MacLachlan A J, Robertson C W, Cross A W and Phelps A D R 2019 *SN Appl. Sci. Adv.* **1** 613
[13] MacLachlan A J, Zhang L, Konoplev I V, Phelps A D R, Robertson C W, MacInnes P, Whyte C G, Ronald K, Cross A W and Henderson M A 2024 *Sci. Rep.* **14** 23906
[14] Ginzburg N S, ZaSlavskii V Y, Malkin A M, Sergeev A S, Zotova I V, Sharypov K A, Shunailov S A, Shpak V G, Ul'masculov M R and Yalandin M I 2022 *Appl. Phys. Lett.* **117** 183505
[15] Ginzburg N S, ZaSlavskii V Y, Malkin A M and Sergeev A S 2017 *Tech. Phys. Lett.* **43** 756–9
[16] Dicke R H 1954 *Phys. Rev.* **93** 1
[17] Bonifacio R, Maroli C and Piovella N 1988 *Opt. Commun.* **68** 369–74
[18] Bonifacio R, McNeil B W J and Pierini P 1989 *Phys. Rev.* A **40** 4467
[19] McNeil B W J, Robb G R M and Jaroszynski D A 1999 *Opt. Commun.* **165** 1–3
[20] Ginzburg N S *et al* 1997 *Nucl. Instrum. Methods Phys. Res.* A **393** 12
[21] Ginzburg N S *et al* 1998 *Tech. Phys. Lett.* **24** 709–11
[22] Ginzburg N S *et al* 1999 *Phys. Rev. E.* **60** 3297–304
[23] McNeil B W J, Robb G R M and Jaroszynski D A 1999 *Opt. Commun.* **163** 4–6
[24] Jaroszynski D A, Wiggins S M, McNeil B W J, Robb G R M, Aitken P, Phelps A D R, Cross A W and Ronald K 2000 *Nucl. Instrum. Methods Phys. Res.* A **393** 261–266
[25] Yalandin M I *et al* 2000 *IEEE Trans. Plasma Sci.* **28** 5
[26] Korovin S D, Eltchaninov A A, Rostov V V, Shpak V G, Yalandin M I, Ginzburg N S, Sergeev A S and Zotova I V 2006 *Phys. Rev.* E **74** 016501
[27] Ginzburg N S *et al* 2016 *Phys. Rev. Lett.* **117** 204801
[28] Ginzburg N S, Fedotov A, Kuzikov S, Sharypov K, Shpak V, Shunailov S, Vikharev A, Yalandin M and Zotova I 2023 *Phys. Rev. Accel. Beams* **26** 060401
[29] Feng J *et al* 2018 *IEEE Trans. Electron Devices* **65** 2156–63
[30] MacLachlan A J, Phelps A D R, Robertson C W, MacInnes P, Whyte C R and Ronald K 2024 Data underpinning this publication is openly available from the University of Strathclyde KnowledgeBase at (https://doi.org/10.15129/e5d23ee5-4208-4428-83a2-69494c39a459)